



NUMERICAL MODELING OF HYDRODYNAMIC IRRIGATION CHANNELS WITH PRESENCE OF SKEWED BOX-CULVERT

Israel Enrique Herrera Díaz^{1*}; Alfredo Márquez Herrera¹; Edith Alejandra Gamiño Ramírez²

¹ Universidad de Guanajuato, Campus Irapuato-Salamanca DICIVA-DIA. Ex Hacienda El Copal, Km. 9. Carretera Irapuato-Silao, C.P. 36500. Irapuato, Guanajuato, México.

eherrera@ugto.mx (*Autor de correspondencia)

² Universidad de Guanajuato, Campus Celaya-Salvatierra DCSI-DEC. Av. Ing. Javier Barrios Sierra N° 201 Esq. Av. Baja California, Ejido de Santa María del Refugio, C.P. 38110. Celaya, Guanajuato, México.

Abstract

The box-culvert in irrigation channels, they are found at road crossings, control works such as gates and intake work. The importance of studying these structures lies in the hydrodynamic behavior of the channels in the rainy season, since they have been detected on free surface elevations due to blockages due to poor design. A numerical model was applied to estimate the hydrodynamic field in open channel with skewed box-culvert in irrigation channels in Mexico, for which purpose the calculation of the three-dimensional velocity field with presence of hydraulic control structures. The numerical method was developed using the Navier-Stokes equations in free surface flow, in cartesian coordinates; use the hypothesis of hydrostatic pressure and considering the postulates of Reynolds, the solve was done by an element finite method. A comparison of the model developed with the Flow3D software was made, where the results between the commercial and the developed model shown an RMSE (Root-Mean-Square Error) of 4.8. Three numerical scenarios were calculated including different alternatives and its behavior at the entrance, interior and exit of the water flow in the construction to determine which is the best option to be used on the skewed multi barrel crossings. In order to accomplish this, a variable slope channel and 1: 60 scale models of box culverts with 10, 22 and 45 degrees of skewness were used. The results observed in the multi-eyed box culverts were favorable, since the speed spans are low increase inside and outside of them, which favors the hydrodynamic behavior and minimize the accumulation of sediment into structure in the channel; another noteworthy fact is that at 45 skewed degrees there is a higher speed, which reduces an upstream hydraulic jump and favors circulation through reductions and control works.

Keywords: Open channel, free flow fluid, Navier-Stokes equations.



Introduction

Sudden increases in water levels in irrigation canals are usually caused by strong or excessive rainfall in a short period of time. Is it so one of the most dangerous weather-related natural phenomena, disasters in the world, and can create dangers situations for people and cause great damage to the property.

In the construction of land roads, flow regulation gates principally and any type of crossing with an irrigation channel, it becomes recommendable to install culverts that, due to their hydraulic characteristics, the loading capacity of the soil where they are built, the slope of the land and their filling conditions may have different geometries and dimensions, allow to provide a flow speed without obstructions or alterations when It leaves a regulation work, bridge or gauging area (Alhinai *et al.*, 2011).

On the other hand, there is little research related to the shape and distribution in culverts and their effect on the characteristics downstream scour. Some works have focused on discussing the hydrodynamic behavior through box culvert on the surface of the water and undermine numerically. They have developed a hydrodynamic and sediment transport model investigated for this purpose using FLOW 3D v11.1.0. Different construction scenarios of the box culvert have been studied. The results obtained using the FLOW 3D program was able to accurately simulate downstream scour Sewer box. Velocity distribution, maximum scour depth and water depth for special cases have been plotted and compared (Nesreen *et al.*, 2020).

A poorly designed culvert may destroy the hydraulic structures from upstream to downstream, which could eventually result in structural failures (Ruike *et al.* 2019). Extensive experimental work had been conducted in the past to investigate the culvert flow at the outlet of culverts. An open-source software, OpenFOAM was applied to simulate the culvert flow under different flow and blockage conditions. The model was validated using a previous experimental measurement. In total, three cases were tested and compared to investigate the impact of blockage on culvert flow. It showed that different blockage scenarios have a strong impact on the flow distribution inside the culvert. With the blockage extending into the culvert, the velocity profile changes significantly comparing to the blockage at the outlet only. With the same extending length, a larger blockage ratio can generate a larger flow re-distribution (Ruike *et al.* 2019).

Other works studied the hydrodynamics of box culverts configured with smooth, uneven and unique roughness, numerically investigated with three-dimensional (3D) computational fluid dynamics (CFD) modeling. Zhang *et al.* (2018), showed results and validation tests they systematically performed against detailed physical data sets, for flow conditions corresponding to flows lower than design. In the study, the authors report that the models were more successful in reproducing the flow characteristics more important than producing quantitative matches with the experimentally obtained velocity profiles, due to inaccuracies in the grid and wall configuration modeling. However, the models were more informative in assessing the distinctive roughness behaviors responsible for the



generation of low-speed zones. Overall, the study acknowledges that current experience suggests a hybrid approach that combines both Numerical and experimental methods for future culvert design optimizations.

A comprehensive verification and validation of the CFD modeling model is more critical as it requires a set of detailed physical data to systematically compare physical and numerical quantities of interest.

In Mexico box culverts are commonly used for their very large hydraulic capacity and its support of large embankments, which makes them ideal for low resistance soils (Herrera *et al.*, 2015).

Sometimes these constructions are not normal to the axis of the road, in those cases, the crossing formed by the natural trajectory of the stream and the road's axis the construction of skewed works becomes necessary.

In the construction of multi barrel box culverts there are two alternatives: the use of prefabricated concrete box culverts and the construction of on-site culverts, the on-site construction respects within its own system of walls and slabs the skewness of the drainage system with the road, constructing in the end of each wall a protection structure; in the cases of the use of prefabricated box culverts involves placing lines of them following the direction of the stream, each line of box culverts adjacent to one another has its own pair of walls that also follow the skewness of the stream with the axis of the road.

The main objective of this work was to study the behavior of the flow in open irrigation channels with the presence of skewed box culverts, in order to know the effects of plugging, hydraulic jumps and backwaters that alter the volumetric measurement to the irrigation modules.

The results of the hydrodynamic calculation correspond to a stable field and converged in time (Rodriguez *et al.*, 2014), which indicates that the velocity fields and their turbulent parameters can be assumed as constants, but with an important spatial variation.

Materials and Methods

Physical laboratory model

The laboratory channel (figure 1) with variable slope and constant rectangular section with a length of 2.32 m by 0.25 m wide and 0.18 m high, has a 22-liter channel feed tank, a 2 hp pump and a storage tank. of 90 liters.

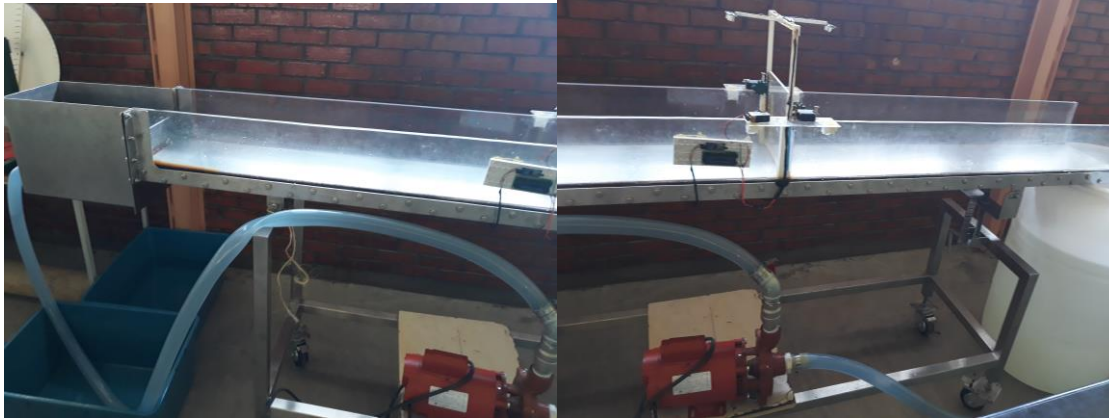


Figure 1. Open channel laboratory

The walls of the channel are made of acrylic sheet 0.012 m thick, and the gate is made of the same material with a thickness of 0.006 m, 0.24 m wide and 0.15 m high, which was in the middle of the length of the channel. In order to avoid oscillations caused by the inlet and outlet weirs. The gate (figure 2) has a weight of 0.346 kg including the plastic chains that serve as a fastening for the servo motors in opening and closing it.



Figure 2. Acrylic electro-gate in the channel

The channel has a weir with a watery crest made of stainless-steel sheet located at the outlet of the feed tank to the channel with a height of 0.076 m and a base of 0.25 m. The outlet of the channel to the storage tank can be with or without a spillway. The bottom of the channel is made of stainless-steel sheet with a thickness of 0.006 m and for which a roughness coefficient of 0.020 was assigned.

The physical scale open channel: the flow rate was 0.0019 m³/s, slope 0.006 and three skewed multi barrel crossings with 0, 10, 22 and 45 degrees (figure 3).

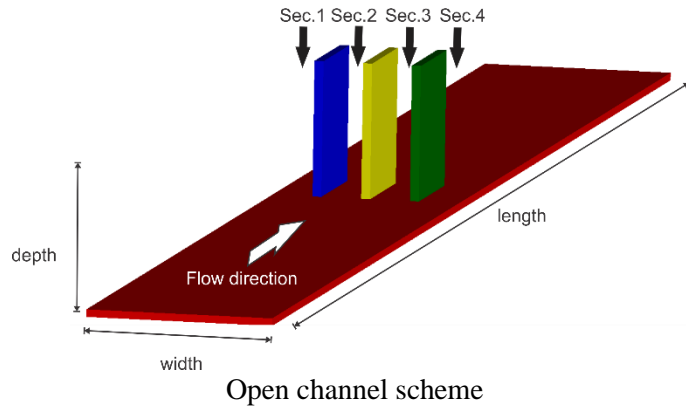


Figure 3. Open channel domain

Governing equations

The system of equations used to describe the velocity fields and the free surface variations are the shallow-water equations (Herrera *et al.* 2015). In order to solve the equations, two approximations are used. The first one is the hydrostatic approximation ($\partial P/\partial z = -\rho_0 g$), where P is the pressure, ρ_0 is the reference density, g is the acceleration due to gravity and z denotes the reference vertical plane. This approximation is valid when the horizontal length scale is much greater than the vertical length scale. This is the main condition for the shallow-water assumption. The second assumption is the Boussinesq approximation, where density is considered constant in all terms of the conservation of momentum equations except for the gravitational term.

By considering the above approximations and after turbulent averaging, governing equations for the velocity components (eqs. 1 - 3) have the following form (Herrera *et al.* 2015):

$$\frac{\partial \bar{u}}{\partial t} + \bar{u} \frac{\partial \bar{u}}{\partial x} + \bar{v} \frac{\partial \bar{u}}{\partial y} + \bar{w} \frac{\partial \bar{u}}{\partial z} = -\frac{1}{\rho_0} \frac{\partial \bar{P}}{\partial x} - \frac{\partial \bar{u}'u'}{\partial x} - \frac{\partial \bar{u}'v'}{\partial y} - \frac{\partial \bar{u}'w'}{\partial z} + f\bar{v} \quad (1)$$

$$\frac{\partial \bar{v}}{\partial t} + \bar{u} \frac{\partial \bar{v}}{\partial x} + \bar{v} \frac{\partial \bar{v}}{\partial y} + \bar{w} \frac{\partial \bar{v}}{\partial z} = -\frac{1}{\rho_0} \frac{\partial \bar{P}}{\partial y} - \frac{\partial \bar{v}'u'}{\partial x} - \frac{\partial \bar{v}'v'}{\partial y} - \frac{\partial \bar{v}'w'}{\partial z} - f\bar{u} \quad (2)$$

$$\frac{\partial \bar{u}}{\partial x} + \frac{\partial \bar{v}}{\partial y} + \frac{\partial \bar{w}}{\partial z} = 0, \quad (3)$$

where t is the time, \bar{u} , \bar{v} and \bar{w} are the time-averaged velocity components, and u' , v' and w' are the corresponding fluctuating components, in the x -, y - and z -directions, respectively. The parameter f is the Coriolis parameter defined by $f = 2\Omega \sin \varphi$, where Ω is the rotation rate of the Earth and φ is the latitude. By integrating the continuity

equation (3) (Herrera *et al.* 2015), over the water depth and by using a kinematic condition at the free surface, leads to the following free surface equation (eq. 4):

$$\frac{\partial \bar{\eta}}{\partial t} + \frac{\partial}{\partial x} \left(\int_{-h}^{\eta} \bar{u} dz \right) + \frac{\partial}{\partial y} \left(\int_{-h}^{\eta} \bar{v} dz \right) = 0 \quad (4)$$

where the water depth h and the time-averaged water surface elevation $\bar{\eta}$ are measured from a reference level or from the undisturbed water surface.

The hydrostatic condition (eq. 5) lets the following definition of pressure (Herrera *et al.* 2015):

$$\bar{P} = g \int_z^{\eta} \rho dz + P_{atm} \quad (5)$$

where P_{atm} is the atmospheric pressure. By applying the Leibnitz integration rule in (5), the pressure terms of (1) and (2) can be written as (Broomans, 2003) in eqs. (6 and 7):

$$-\frac{1}{\rho_0} \frac{\partial \bar{P}}{\partial x} = -\frac{\rho g}{\rho_0} \frac{\partial \bar{\eta}}{\partial x} - \frac{g}{\rho_0} \int_z^{\eta} \frac{\partial \rho'}{\partial x} dz - \frac{1}{\rho_0} \frac{\partial P_{atm}}{\partial x} \quad (6)$$

$$-\frac{1}{\rho_0} \frac{\partial \bar{P}}{\partial y} = -\frac{\rho g}{\rho_0} \frac{\partial \bar{\eta}}{\partial y} - \frac{g}{\rho_0} \int_z^{\eta} \frac{\partial \rho'}{\partial y} dz - \frac{1}{\rho_0} \frac{\partial P_{atm}}{\partial y} \quad (7)$$

where $\rho' = \rho - \rho_0$ is the anomalous density. In this way, the horizontal pressure gradient is described in (6) and (7) by the variation of the free surface through the barotropic term (the first term on the right-hand), by density differences in horizontal direction through the baroclinic term (the second term) and the atmospheric pressure acting on the free surface (the last term). If density is considered constant and the atmospheric pressure contribution is neglected, the horizontal pressure gradients will reduce to barotropic term.

A state equation (eq. 8) is used to compute density variations and is defined as (UNESCO, 1981):

$$\rho(\bar{P}, \bar{T}, \bar{S}) = \frac{\rho_0}{\left(1 - \frac{\bar{P}}{k_p}\right)}, \quad (8)$$

where k_p is a coefficient function of pressure, temperature and salinity. The formulation to compute the value of k_p can be found in UNESCO (1981).

In summary, hydrodynamic is described by four unknowns, $\bar{u}, \bar{v}, \bar{w}$ and $\bar{\eta}$, computed through (1) - (4), respectively, and thermodynamic is defined by ρ, \bar{T} and \bar{S} , computed through (8) - (10), respectively. Pressure appearing in (8) is the hydrostatic one and can be estimated at any time (Herrera *et al.* 2015).

Turbulence modeling

The Reynolds stress correlations $\overline{u'u'}, \overline{u'v'}, \overline{u'w'}, \dots, \overline{v'w'}$ of (1) and (2), are computed by using a zero-equations turbulence model (Herrera *et al.* 2015). Such models replace these correlations by the product of the kinematic eddy viscosity ν_E and the mean strain-rate tensor as follows in eqs (11 and 12):

$$-\frac{\partial \overline{u'u'}}{\partial x} - \frac{\partial \overline{u'v'}}{\partial y} - \frac{\partial \overline{u'w'}}{\partial z} = \frac{\partial}{\partial x} \left(2\nu_E \frac{\partial \bar{u}}{\partial x} \right) + \frac{\partial}{\partial y} \left[\nu_E \left(\frac{\partial \bar{u}}{\partial y} + \frac{\partial \bar{v}}{\partial x} \right) \right] + \frac{\partial}{\partial z} \left(\nu_E \frac{\partial \bar{u}}{\partial z} \right) \quad (11)$$

$$-\frac{\partial \overline{v'u'}}{\partial x} - \frac{\partial \overline{v'v'}}{\partial y} - \frac{\partial \overline{v'w'}}{\partial z} = \frac{\partial}{\partial y} \left(2\nu_E \frac{\partial \bar{v}}{\partial y} \right) + \frac{\partial}{\partial x} \left[\nu_E \left(\frac{\partial \bar{u}}{\partial y} + \frac{\partial \bar{v}}{\partial x} \right) \right] + \frac{\partial}{\partial z} \left(\nu_E \frac{\partial \bar{v}}{\partial z} \right) \quad (12)$$

where kinematic eddy viscosity has turbulent and molecular components such that $\nu_E = \nu_t + \nu$, respectively. The turbulent viscosity coefficient ν_t is then computed through the following mixing length model (Stansby, 2003) by eq. (13):

$$\nu_t = \left(l_h^4 \left[2 \left(\frac{\partial \bar{u}}{\partial x} \right)^2 + 2 \left(\frac{\partial \bar{v}}{\partial y} \right)^2 + \left(\frac{\partial \bar{v}}{\partial x} + \frac{\partial \bar{u}}{\partial y} \right)^2 \right] + l_v^4 \left[\left(\frac{\partial \bar{u}}{\partial z} \right)^2 + \left(\frac{\partial \bar{v}}{\partial z} \right)^2 \right] \right)^{1/2} \quad (13)$$

where the vertical length scale $l_v = \kappa(z - z_b)$ for $(z - z_b)/\delta < \lambda/\kappa$ and $l_v = \lambda\delta$ for $\lambda/\kappa < (z - z_b)/\delta < 1$, κ is the von Kármán constant typically 0.41, $(z - z_b)$ is the distance from the wall, δ is the boundary-layer thickness and λ is a constant, typically 0.09. In the case of shallow-water flows, due to a steady current, the boundary-layer thickness may be assumed to be equal to the water depth h (Stansby, 2003). The horizontal length scale is usually different than the vertical length scale, and the simplest assumption is to assume direct proportionality defined by $l_h = \beta l_v$ (Stansby, 2003). The constant β must be determined experimentally. For parallel flow cases (or near parallel), eddy viscosity reverts to its standard boundary-layer form. With $l_h = l_v$, it reverts to its correct mathematical three-dimensional form (with negligible vertical velocity) (Herrera *et al.* 2015).

Free surface and bottom conditions

The shear stress at the free surface is specified by the prescribed wind stresses τ_{ox} and τ_{oy} (eqs. 14-15) (Herrera *et al.* 2015):

$$v_t \left. \frac{\partial \bar{u}}{\partial z} \right|_{surface} = \tau_{\omega x} \quad (14)$$

$$v_t \left. \frac{\partial \bar{v}}{\partial z} \right|_{surface} = \tau_{\omega y} \quad (15)$$

where $\tau_{\omega x} = C_{\omega} \rho_a \bar{\omega}_x |\bar{\omega}_x|$ and $\tau_{\omega y} = C_{\omega} \rho_a \bar{\omega}_y |\bar{\omega}_y|$, ρ_a is the air density, and $\bar{\omega}_x$ and $\bar{\omega}_y$ are the mean wind velocity components. The wind-drag coefficient C_{ω} is computed by the Garratt's formula $C_{\omega} = (0.75 + 0.067\bar{\omega}) \times 10^{-3}$ (Garratt, 1977), where $\bar{\omega}$ is the main magnitude of wind velocity vector. The wind velocity is usually taken at 10 m above the free surface.

The shear stress at the bottom is given by the bottom stress defined in terms of the velocity components by using the Manning-Chezy formula such as:

$$v_t \left. \frac{\partial \bar{u}}{\partial z} \right|_{bottom} = \frac{g \sqrt{\bar{u}^2 + \bar{v}^2}}{C_z^2} \bar{u} \quad (16)$$

$$v_t \left. \frac{\partial \bar{v}}{\partial z} \right|_{bottom} = \frac{g \sqrt{\bar{u}^2 + \bar{v}^2}}{C_z^2} \bar{v} \quad (17)$$

where C_z is the Chezy friction coefficient. The velocity components are taken from values of the layer adjacent to the sediment-water interface.

Numerical model

The numerical model was worked with a finite difference element (Figure 4) the first scenario contained to zero degrees of skewness; the second scenario to ten degrees of skewness; the third scenario to twenty-two degrees of skewness; and the last scenario to forty-five degrees of skewness were simulated with time increments of $\Delta t = 0.01$ s and total time of 1500 s.



Scenario 1: Zero degrees of skewness



Scenario 2: Ten degrees of skewness



Scenario 3: Twenty-two degrees of skewness



Scenario 4: Forty-five degrees of skewness

Figure 4. Numerical mesh in different degrees of skewness

The hydrodynamic model was used to generate the velocity field corresponding to end time simulation, taking as force the magnitude of flow rate of 0.0019 m³/s and slope of 0.006 in all scenarios.

Initial condition and boundary conditions

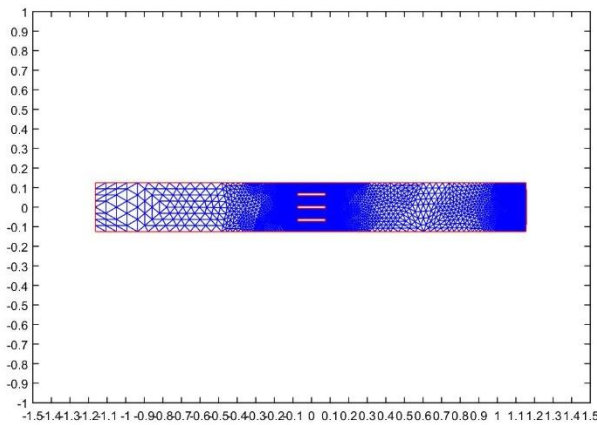
The initial and boundary conditions for numerical simulation are described in table (1).

Table 1. Initial and boundary condition

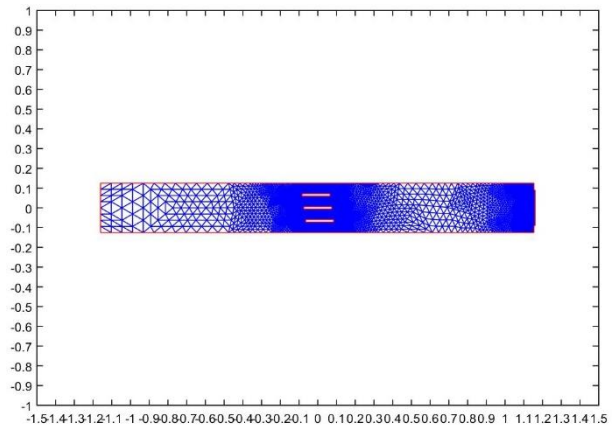
Initial condition		Boundary condition	
Time simulation:	1500 s	Walls and bottom:	$du/dt = dv/dt = 0$
Time step:	0.1 s	Free surface:	$dn/dt = 0$
Flow rate:	0.0019 m ³ /s	Turbulence model:	Mixing length
Velocity fields:	$du/dt = dv/dt = 0$	Out flow:	Dirichlet condition

Results and Applications

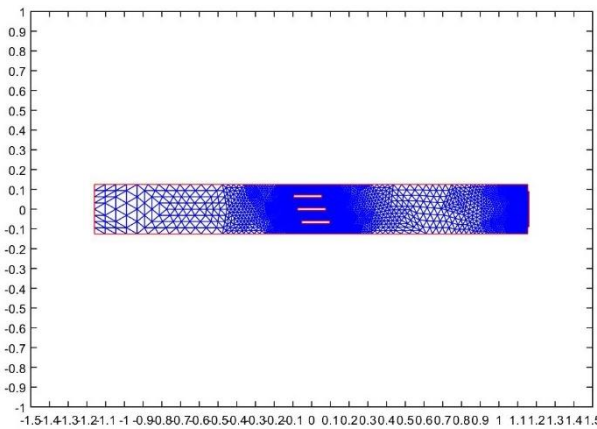
The numerical model was worked with a mesh in finite elements (Figure 5) the first scenario contained 8986 nodes and 17280 triangles to zero degrees of skewedness; the second scenario contained 7730 nodes and 14816 triangles to ten degrees of skewedness; the third scenario was 2034 nodes and 3736 triangles to twenty-two degrees of skewedness; and the last scenario was 8178 nodes and 15712 triangles to forty-five degrees of skewedness were simulated with increments of $\Delta t = 0.01$ s and total time of 1500 s.



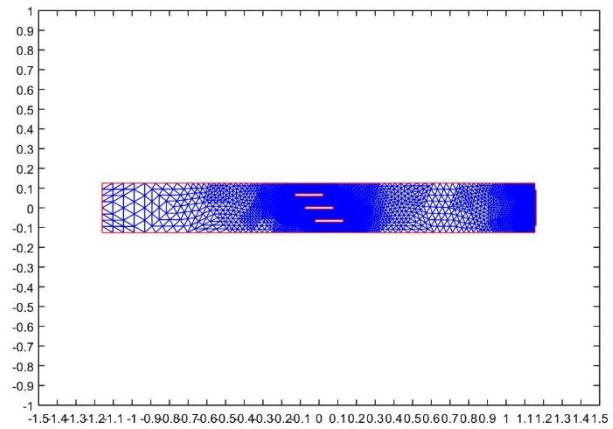
Scenario 1: zero degrees of skewedness



Scenario 2: ten degrees of skewedness



Scenario 3: twenty-two degrees of skewedness

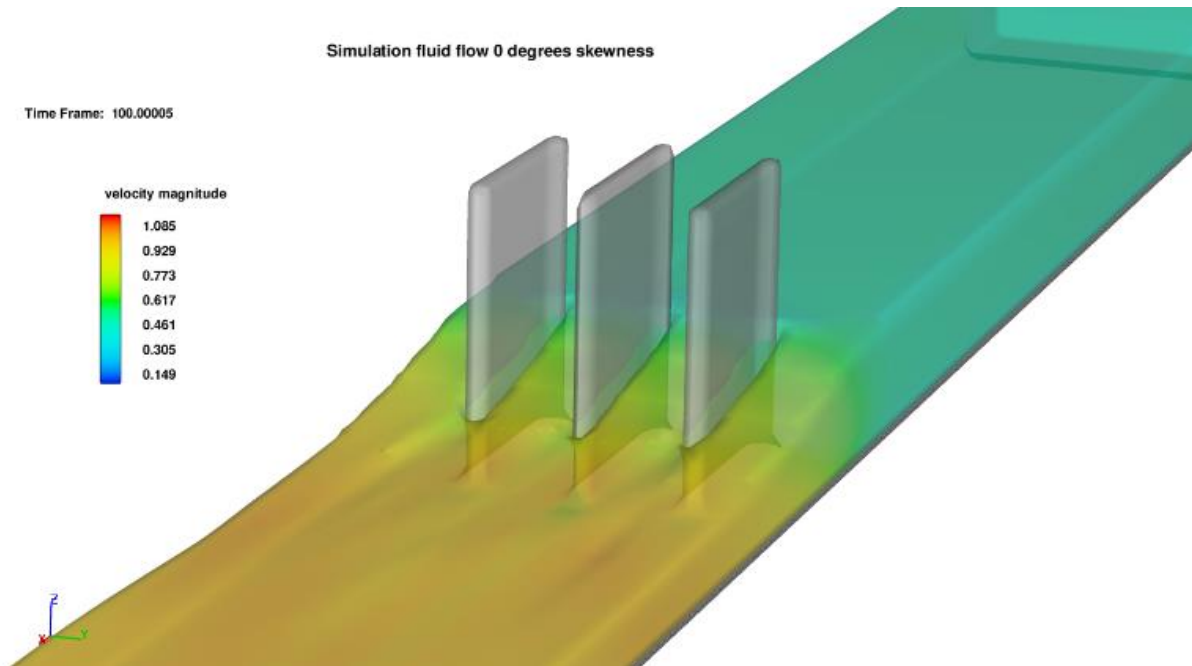


Scenario 4: forty-five degrees of skewedness

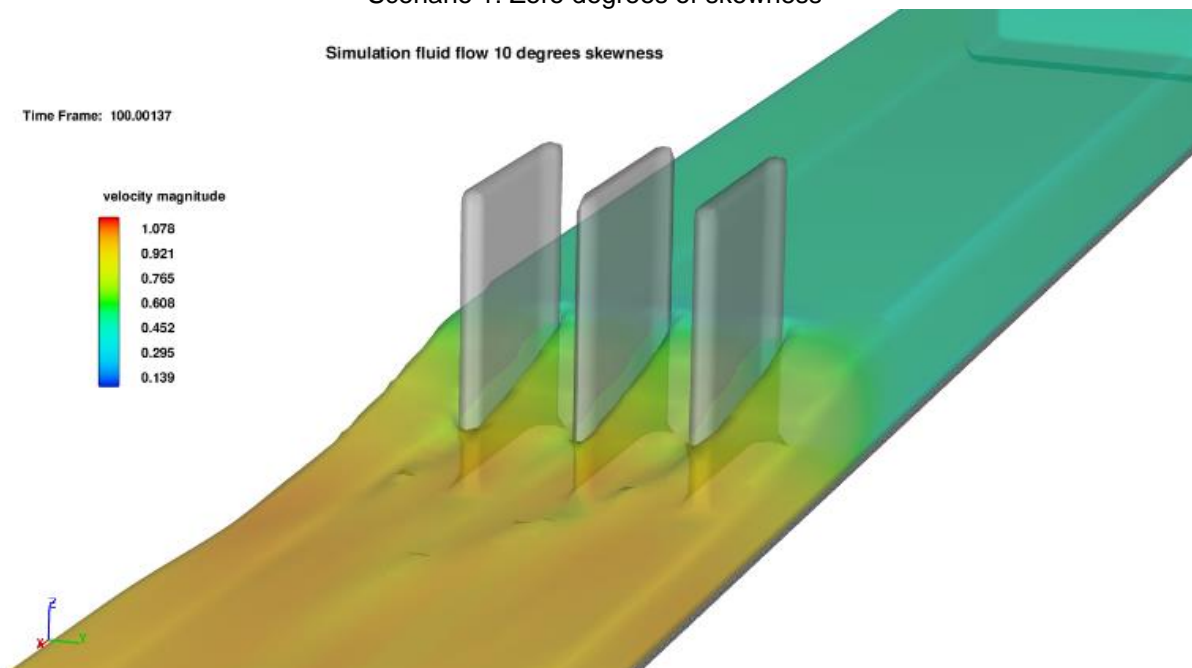
Figure 5. Finite element mesh in different degrees of skewedness

The hydrodynamic model was used to generate the velocity field corresponding to 1500 s., taking as force the magnitude of flow rate in all scenarios.

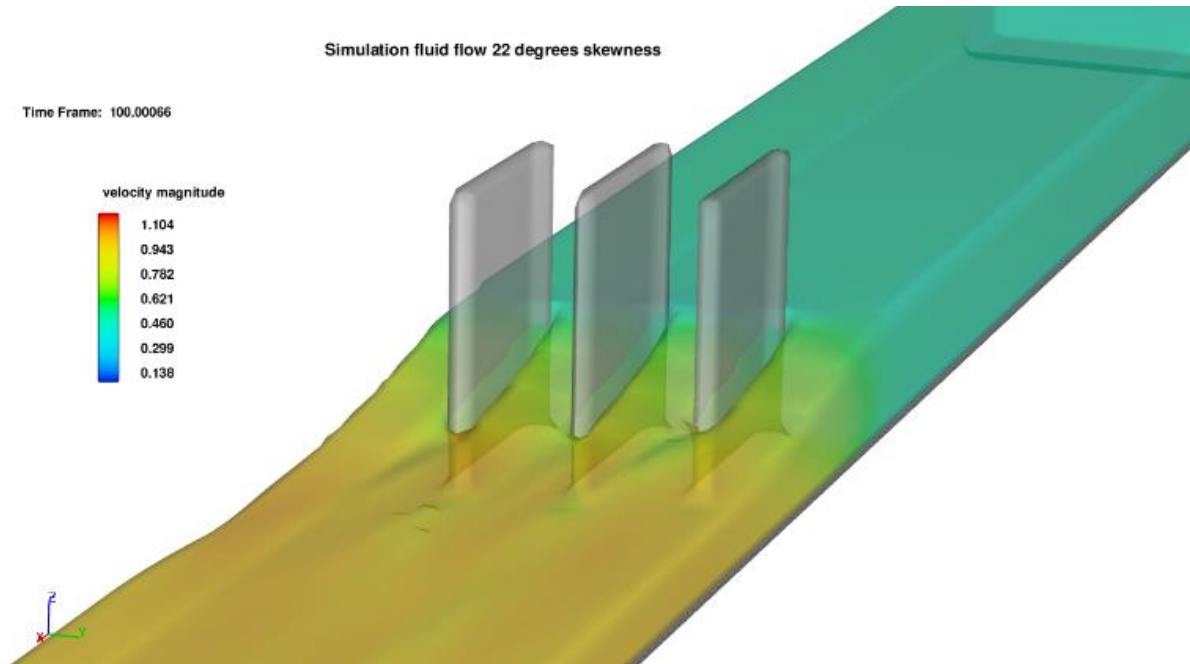
The results of hydrodynamical field are showed in Figure (6) for each scenario, they show that the location and geometry of the culverts make it possible to increase the flow of the channel by an average of 8% and reduce the level of the free surface or hydraulic depth by 15% of the initial value before the culverts.



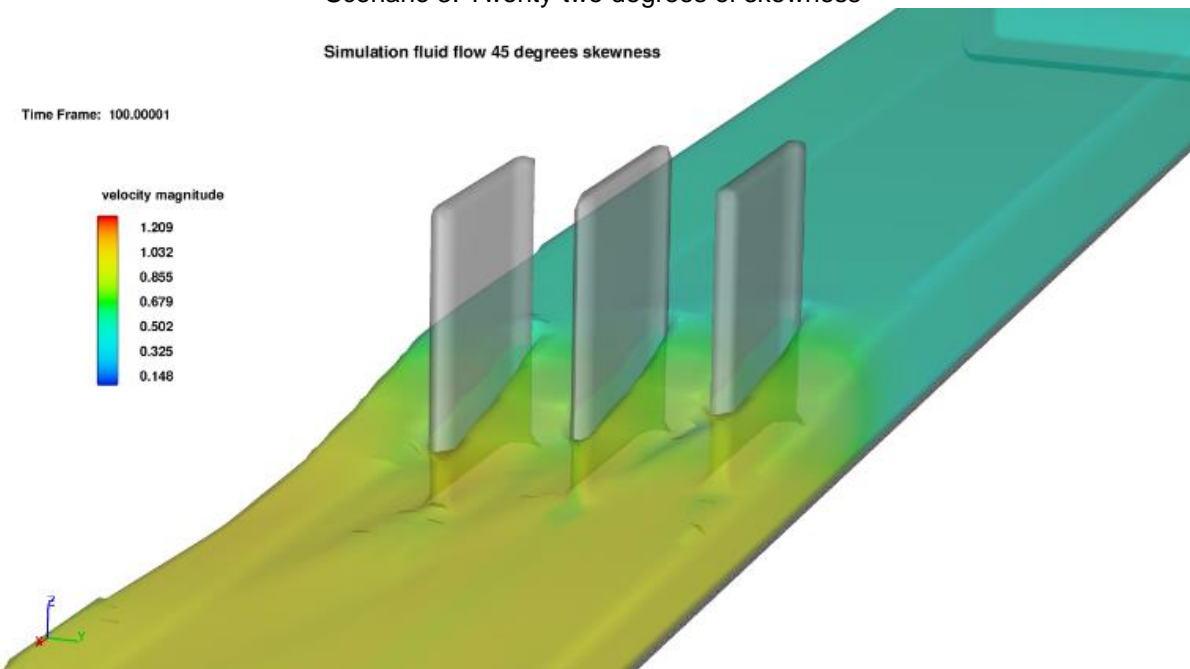
Scenario 1: Zero degrees of skewness



Scenario 2: Ten degrees of skewness



Scenario 3: Twenty-two degrees of skewness



Scenario 4: Forty-five degrees of skewness

Figure 6. Hydrodynamical field and velocity magnitude in m/s

As can be seen in the results of the velocity field, the increase in velocity allows the removal of sediment material deposited on the bottom, as well as other elements that, due to drag, accumulate on overpasses or bridges. The geometry and placement of the culverts at 45 degrees allows a better distribution of the flow through them. In the Figure 7, the results of the behavior of the hydrodynamic field in X-Y plane are

presented, it is observed that the velocity magnitude had change in each scenario, especially near to the box-culvert.

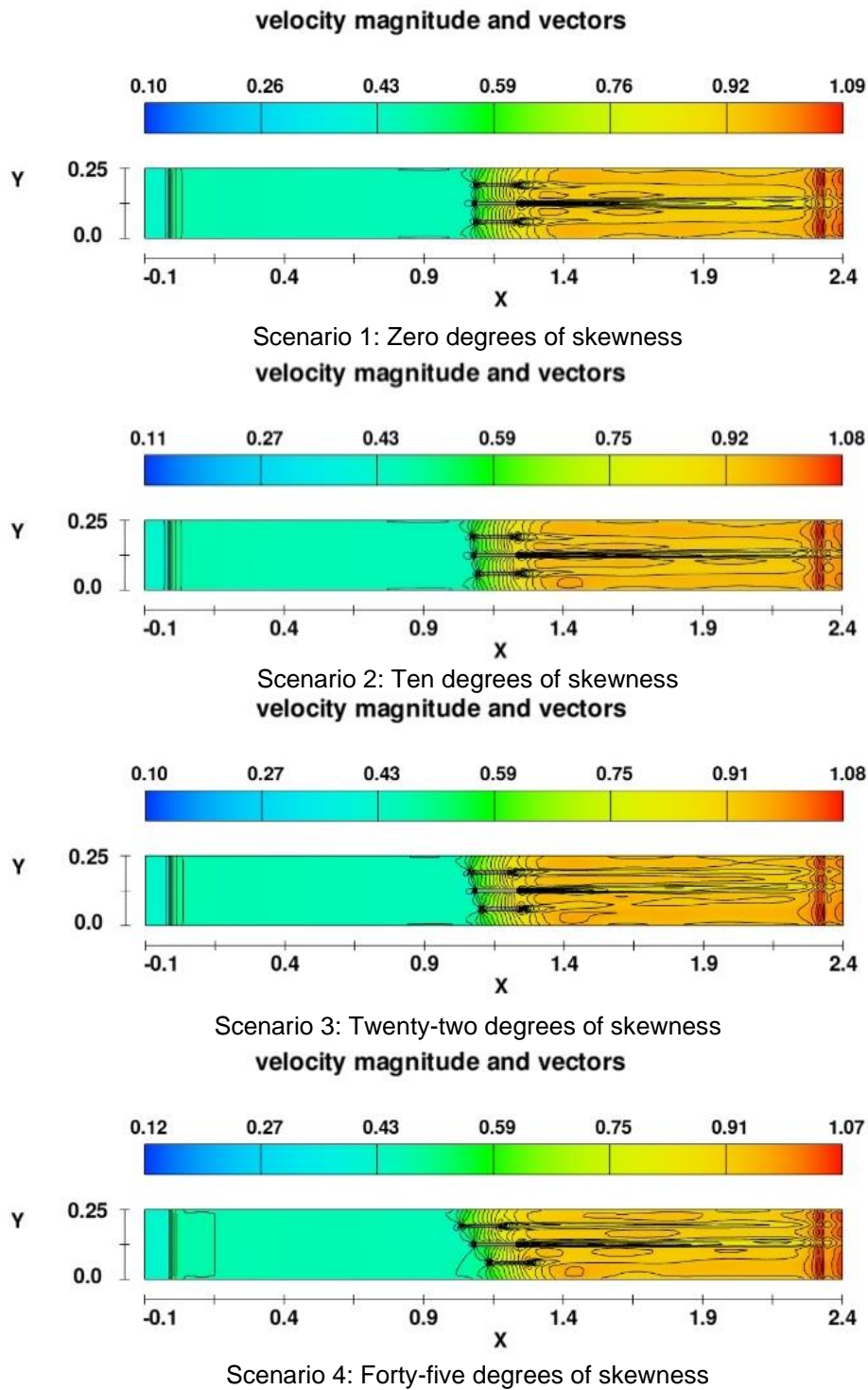
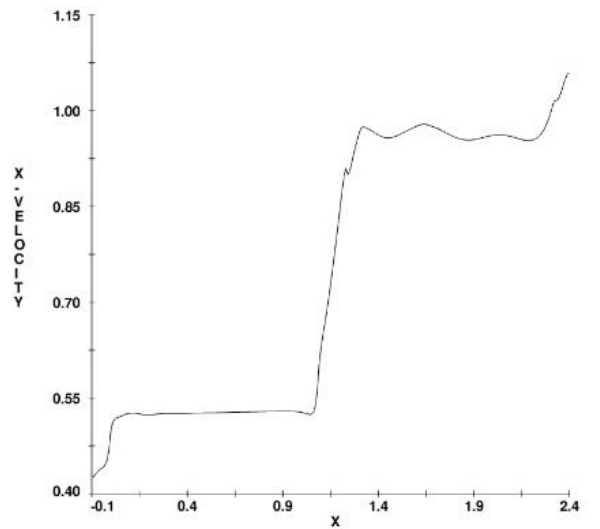


Figure 7. Velocity magnitude (m/s) and streamlines

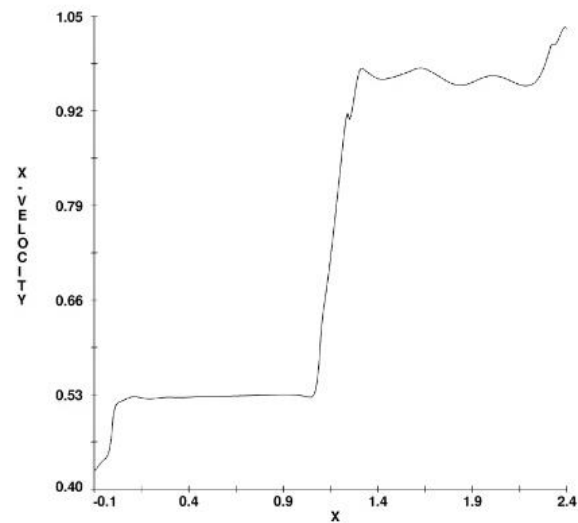
The differences observed are caused by the degrees of skewness, it is observed that the magnitude and behavior of the hydrodynamic field after the box-culverts are similar, where the turbulence occurs with greater magnitude in the center of the channel.

It is important to note that the higher the degree of skewness, the turbulence generated by the geometry is reduced at the outlet; however, at the inlet it can cause recirculation in the first structures and greater agitation in the latter, as observed in Figure (7) scenario 4. Numerical modeling allows flow behavior under controlled conditions, where the flow rate is constant, and it is observed that the changing conditions of the structures at different degrees of skewness have a significant influence on the velocity field.

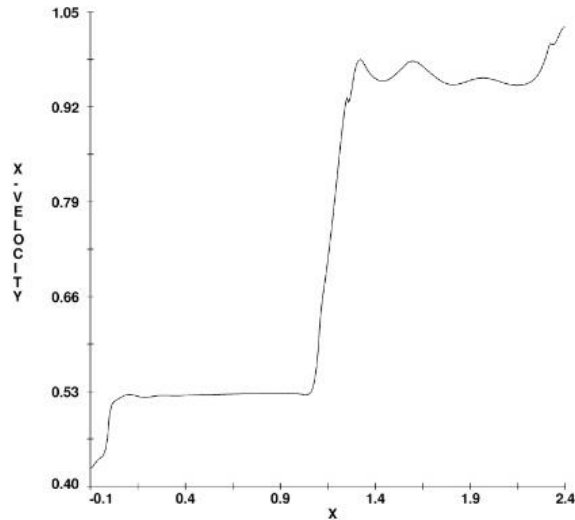
And in the figure (8), observed the mean velocity profile in the longitudinal direction in each scenario in the center of channel.



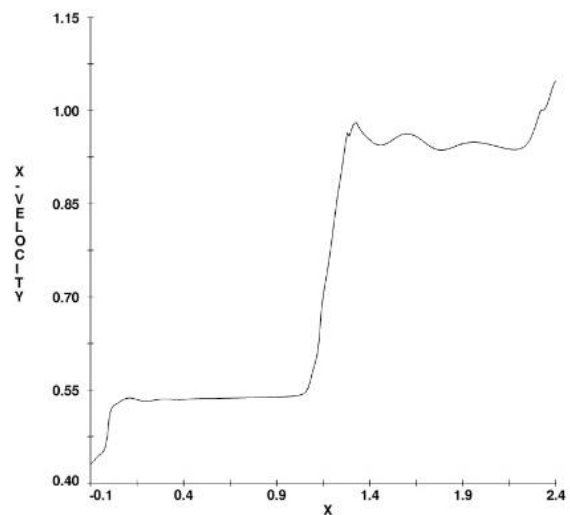
Scenario 1: Zero degrees of skewness



Scenario 2: Ten degrees of skewness



Scenario 3: Twenty-two degrees of skewness



Scenario 4: Forty-five degrees of skewness

Figure 8. Velocity profile in the center of the channel (m/s)

The velocity profiles show that the increase in the magnitude of the velocity is a function of the degree of skewness that has the configuration, and the behavior of the velocity field is similar in all scenarios, the only difference is the magnitude of the velocity at the exit of the box-culvert.

The comparison of the velocity field with the physical model was carried out qualitatively, where in a future work using a PIV meter, the magnitudes of velocities in different sections of the channel will be compared and the results obtained from the numerical model will be validated.



Conclusion

The results of the numerical modelling of hydrodynamics in the different scenarios show the importance of geometry in the design of the box-culverts; where the most common angles were those studied in this work.

The magnitude and increase of the flow velocity when leaving the box-culverts is increased by 12% with respect to the scenario without skewness, where the most unfavourable angle is 22 degrees because from this value, the velocity increases and therefore the appearance of vortices at the exit of the box-culverts.

It was noted that, as the output velocity increases, there is the possibility of the appearance of undercutting or erosion of the bottom, where as a recommendation, the use of box-culvert with a 22- and 45-degree swamp should be taken carefully in the designs of irrigation channels.

In general, the behavior of the hydrodynamic field at the end of the simulation time under controlled conditions such as the flow and slope of the channel, allows the irrigation channels to be designed under extreme conditions, as well as the use of computational tools and scale models in laboratories, allow to obtain reliable results for the design of structures such as drained sewers, floodgates, flow meters, etc.

Currently, the study is continued through comparison with other numerical models, under different hydraulic and geometric scenarios, as well as the use of physical experimentation in scale models to reproduce damming conditions and control elements or structures.

References

- Alhinai S., Takashi H., Hidekazu S. (2011). Numerical modeling of unsteady flow Around a box culvert and its Verification. *Journal of Japan Society of Civil Engineers, Ser. Vol. 67, N°4*, pp 199-204.
- Broomans, P. (2003). Numerical accuracy in solutions of the shallow-water equations. Master thesis, TU Delf & WL, Delf Hydraulics.
- Garratt, J. R., (1977). Review of drag coefficients over oceans and continents, *Monthly Weather Review*, Vol. 105, pp 915-929.
- Herrera I.E., Rodríguez C., Couder C., Gasca J.R. (2015). Modelación numérica hidrodinámico-hidrológica en zonas de inundación con presencia de infraestructura, *Tecnología y Ciencias del Agua*, Vol. VI, Num. 1 Ene-Feb., pp. 139-152.
- Nesreen T., Maged M., Atef A., Ismail F. (2020). Numerical investigation of scour characteristics downstream of blocked culverts. *Alexandria Engineering Journal*, 59, 3503–3513.



Rodríguez C., Couder C., Flores E., Herrera I.E., Cisneros R. (2014). Modelling shallow water wakes using a hybrid turbulence model, *Journal of Applied Mathematics*, Vol. 1, pp.1-10.

Ruike Z., Yee-Chung J. and Peng W. (2019). Numerical simulation of culvert flow using OpenFoam. *E-proceedings of the 38th IAHR World Congress*, Panama City, Panama.

Stansby, P. (2003). A mixing-length model for shallow turbulent wakes. *Journal of Fluid Mechanics*, Vol. 495, pp. 369-384.

UNESCO (1981). Background papers and supporting data on the International Equation of State of seawater 1980. *UNESCO technical papers in marine science*, 38, pp. 192.

Zhang G., Chanson H. (2018). Numerical Investigations of Box Culvert Hydrodynamics with Smooth, Unequally Roughened and Baffled Barrels to Enhance Upstream Fish Passage. Hydraulic model report No. CH111/18, University of Queensland, School of Civil Engineering, Brisbane QLD 4072, Australia.